Ocean Sci. Discuss., https://doi.org/10.5194/os-2018-133
Manuscript under review for journal Ocean Sci.
Discussion started: 28 January 2019

Ocean Science Discussions
Open Access

Eddy-induced Track Reversal and Upper Ocean Physical-Biogeochemical Response of Tropical Cyclone Madi in the Bay of Bengal

Riyanka Roy Chowdhury[1], S. Prasanna Kumar[2], Arun Chakraborty[1]

[1]Centre for Oceans, Rivers, Atmosphere and Land Sciences, Indian Institute of Technology Kharagpur, Kharagpur721302, West Bengal, India

[2]CSIR-National Institute of Oceanography, Dona Paula, Goa 403004, India

Correspondence to: S. Prasanna Kumar (prasanna.ocean@gmail.com)

Abstract. The life cycle of the tropical cyclone Madi in the southwestern Bay of Bengal (BoB) during 6th to 12th December 2013 was studied using a suite of ocean and atmospheric data. Madi formed as a depression on 6th December and intensified into a very severe cyclonic storm by 8th December. What was distinct about Madi was its (1) swift weakening from very severe cyclone to a severe cyclone while moving towards north on 9th, (2) abrupt track reversal close to 180-degree in a southwestward direction on 10th, and (3) rapid decay in the open ocean by 12th December while still moving southwestward. Using both in situ and remote sensing data, we show that oceanic cyclonic eddies played a leading role in the ensuing series of events that followed its genesis. The sudden weakening of the cyclone before its track reversal was facilitated by an oceanic cyclonic (cold-core) eddy, which reduced the ocean heat content and cooled the upper ocean through upward eddy-pumping of subsurface waters. When Madi moved over the cyclonic eddy-core, its further northward movement was arrested. Subsequently, the prevailing northeasterly winds assisted the slow moving system to change its track to a southwesterly path. While travelling southwestwards, the system rapidly decayed when it passed over cyclonic eddies near the western boundary of the BoB. Though Madi was a category-2 cyclone, it had a profound impact on the physical and biogeochemical state of the upper ocean. Cyclone-induced enhancement in the chlorophyll *a* ranged from 5 to 7-fold, while increase in the net primary productivity ranged from 2.5 to 8-fold. This enhancement of chlorophyll *a* and net primary productivity was much higher than previous cyclones that occurred in the BoB. Similarly, the CO_2 out-gassing into the atmosphere showed a 3.7-fold increase compared to the pre-cyclone values. Our study points to the crucial role oceanic eddies play in the life cycle of cyclones and their combined impact on upper-ocean biogeochemical changes in the BoB. Eddies are ubiquitous and tropical cyclones occur in the BoB; there is an urgent need to incorporate eddies in models for better prediction of cyclone track and intensity. As cyclone and eddy co-exists in many parts of the world ocean our approach in delineating the upper-ocean biogeochemical changes can be adapted elsewhere.

1 Introduction

The Bay of Bengal (BoB) (Fig. 1) is a tropical sea situated in the eastern part of the northern Indian Ocean. The two most important characteristic features of the BoB are the perennial presence of low salinity waters (30-34 psu) in the upper ocean and the seasonal reversal of atmospheric winds from northeasterly direction between

November and February (5 m/s, northeast or winter monsoon) to southwesterly during June to September (9 m/s, southwest or summer monsoon) (Narvekar and Prasanna Kumar, 2006). This perennial presence of low salinity waters enhances the stability of the upper water column through increased stratification and makes it one of the warmest regions in the Indian Ocean. The BoB is a site of tropical cyclones, which occur usually during pre-monsoon (April-May) and post-monsoon (October-November) periods. Though north Indian Ocean accounts for only 7% of the total number of tropical cyclones that occur worldwide, the frequency of occurrence of cyclones in the BoB is 4-times higher than that in the Arabian Sea (Dube et al., 1997). Each year 3-5 cyclones occur in the BoB, with a primary peak during post-monsoon and a secondary peak in pre-monsoon.

Tropical cyclones in the BoB have been a subject of study by many researchers, which can be broadly classified into those that deal with (1) prediction of track and intensity of tropical cyclone (e.g., Rao et al., 2007; Basu and Bhagyalakshmi, 2010; Srinivas et al., 2013; Kanase and Salvekar, 2014; Das et al, 2016; Prakash and Pant, 2017), (2) air-sea interaction and cooling of sea surface temperature (SST) (e.g., O'Brian et al., 1967; Premkumar et al., 2000; Sadhuram, 2004; Subrahmanyam et al., 2005; Sengupta et al., 2008; McPhaden et al., 2009; Lin et al., 2009; Kotal et al., 2013; Vissa et al., 2013; Mathew et al., 2018), (3) cyclone-induced phytoplankton bloom and chlorophyll enhancement (e.g., Madhu et al., 2002; Vinayachandran et al., 2003; Rao et al., 2006; Patra et al., 2007; Tumula et al., 2009; Sarangi, 2011; Maneesha et al., 2011; Tripathy et al., 2012; Vidya et al., 2017), and (4) eddy-cyclone interaction (e.g., Ali et al., 2007; Lin et al., 2009; Sadhuram et al., 2011; Patnaik et al., 2014).

Though there have been several studies on the tropical cyclone-ocean interaction in the Pacific (typhoon) and the Atlantic (hurricane) that have advanced our understanding about the upper ocean response in terms of cooling of SST and enhancement of chlorophyll (e.g., Chang and Anthes, 1978; Price, 1981; Emanuel, 1999; Babin et al., 2004; Wada and Chan, 2008; Liu et al., 2009; Pun et al., 2011) and cyclone-eddy interaction (e.g., Shay et al., 2000; Jaimes and Shay, 2009; Lin et al., 2011; Yablonsky and Ginis, 2013; Sun et al., 2014), the depth-dependent temperature and chlorophyll response is still poorly understood. It is in this context that the present paper aims at understanding the (1) ocean-atmosphere condition associated with the evolution of cyclone Madi, a category-2 cyclone (Saffir-Simpson scale), during December 2013 in the BoB, its sudden weakening and close to180-degree track reversal before its dissipation, (2) time-evolution of depth-dependent temperature and chlorophyll profiles in the vicinity of cyclone Madi, and (3) cyclone-induced physical and biogeochemical response of the upper ocean.

2 Materials and Methods

2.1 Data

In the present study, the information on cyclone Madi was taken from Indian Meteorological Department (IMD) (http://www.imd.gov.in), while the track information was taken from Unisys Weather (http://weather.unisys.com/hurricanes/search). The daily SST data was taken from Tropflux (Praveen Kumar et al., 2012) (http://www.incois.gov.in/tropflux_datasets/ data/ daily/), while daily sea level anomaly (SLA) along with zonal and meridional geostrophic current data were taken from AVISO

Ocean Sci. Discuss., https://doi.org/10.5194/os-2018-133
Manuscript under review for journal Ocean Sci.
Discussion started: 28 January 2019

(https://www.aviso.altimetry.fr/en/my-aviso.html). The zonal and meridional components of wind at 10 m height were taken from Advanced Scatterometer (ASCAT) level 3 product (Bentamy and Croize-Fillon, 2012) (https://opendap.jpl.nasa.gov/opendap/OceanWinds/ascat/preview/L2/metop_a/12km/contents.html). It is a daily product having a spatial resolution of 0.25 degree latitude by longitude. This has been further used for the calculation of wind stress curl and Ekman pumping velocity (Gill, 1982) as given below:

$$\text{Wind stress curl} = \frac{\partial \tau_y}{\partial x} - \frac{\partial \tau_x}{\partial y} \tag{1}$$

$$\text{Ekman pumping velocity} = -\frac{1}{\rho f}\left(\frac{\partial \tau_y}{\partial x} - \frac{\partial \tau_x}{\partial y}\right) \tag{2}$$

where τ_x, τ_y are the zonal and meridional wind stress components, ρ is the density of sea water with its value taken as 1026 k gm^{-3}, and f is the Coriolis parameter which varies with latitude.

The oceanic heat content (OHC) in the upper 300 m is calculated following Eq. (3):

$$\text{OHC} = \rho c_p \int_{h_2}^{h_1} T(z)\, dz \tag{3}$$

where, ρ is the density of seawater, c_p is the specific heat capacity of sea water taken as 3.87 kJ kg^{-1} K^{-1}, h_1 and h_2 are the lower and upper water depths, and $T(z)$ is the temperature profile measured in Kelvin.

The relative humidity at 500 hpa was taken from NCEP 2 reanalysis daily data having 2.5 degree grid resolution (https://www.esrl.noaa.gov/psd/data/gridded/data.ncep.html) (Kalnay et al., 1996). The daily zonal and meridional components of wind at 850, 500 and 200 hpa having a spatial resolution of 0.5 degree were extracted from NCEP climate forecast system version 2 and used to compute vector wind. Winds at 850 and 200 hpa were used for the calculation of vertical wind shear (Saha et al., 2014) (http://www.ncep.noaa.gov).

In order to gain insight about the time evolution of temperature and chlorophyll in the upper water column in response to the passage of cyclone Madi, we have analyzed the trajectory of two Argo floats (WMO ID 2901288, 2901629) for temperature profiles that were in the vicinity of Track 2 and one Bio-Argo float (WMO ID 2902086) for chlorophyll profiles that was to the right of Track 1 as shown in Fig. 1. Argo/Bio-Argo data were downloaded from Argo CORIOLIS site (http://www.coriolis.eu.org/Data-Products/Data-Delivery/Data-selection).

2.2 Data Processing method of Chlorophyll and net primary production

The satellite-derived daily chlorophyll *a* (Chl-*a*) pigment concentration data and net primary production (NPP) estimated based on vertically generalized productivity model (VGPM) of (Behrenfeld and Falkoswski, 1997) were taken from Moderate Resolution Imaging Spectro-radiometer (MODIS) Aqua Ocean color (https://oceandata.sci.gsfc. nasa.gov/MODISA/). The Level 3 Chl-*a* dataset has a zonal and meridional resolution of 0.05 degree longitude by latitude. From the daily data, weekly composites were calculated.

Ocean Sci. Discuss., https://doi.org/10.5194/os-2018-133
Manuscript under review for journal Ocean Sci.
Discussion started: 28 January 2019

Ocean Science
Discussions
Open Access

In order to determine the net CO_2 flux over southwestern BoB, before, during, and after the passage of the cyclone Madi, pCO_2^{air} data was taken from NOAA ESRL (ftp://aftp.cmd1.noaa.gov/product/ trends/co2/co2_mm_g1.txt). Since the daily pCO_2^{sea} values are not available, the value of climatological air-sea difference in partial pressure of CO_2 was taken from (Takahashi et al., 2009) and the net flux was calculated using the following formula:

$$F = k.a.(pCO_2{}^{sea} - pCO_2{}^{air}) \quad (4)$$

where, *k* denotes the gas transfer velocity, *a* is the solubility of CO_2 in sea water which is dependent on sea surface temperature and salinity (Weiss, 1974) as per the following equations:

$$\ln a = A_1 + A_2\left(\frac{100}{T}\right) + A_3 \ln\left(\frac{T}{100}\right) + S\left[B_1 + B_2\left(\frac{T}{100}\right) + B_3\left(\frac{T}{100}\right)^2\right] \quad (5)$$

The gas-transfer velocity "k" is calculated using wind speed following (Wanninkhof, 1992) by using the formula

$$k(cm\ h^{-1}) = \Gamma \cup^2 \left(\frac{S_c}{660}\right)^{-1/2} \quad (6)$$

where Γ is the scaling factor and its value of 0.26 is taken from (Takashashi et al., 2009), while $\cup$ is the wind speed. S_c is the Schimidt number (kinematic viscosity of water/diffusion coefficient of CO_2 in water), the value of which is 660 for CO_2 in seawater at 20°C and is a function of temperature and is computed as:

$$S_c = A - BT + CT^2 - DT^3 \quad (7)$$

For the values of the constants A, B, C and D refer (Weiss, 1974; Wanninkhof, 1992).

We have divided the study region into Box A, Box B, Track 1, Track 2 and Box abcd. See Fig.1 for the location of these sub-regions.

2.3 Origin, evolution and decay of the cyclone Madi

On 30th November 2013, as per the Indian Daily Weather Report of India Meteorological Department (IMD), a low pressure system was formed over the southwestern part of the BoB (Fig. 1) and slowly intensified into a depression (the classification of intensity of the system is based on IMD, http://imd.gov.in/section/nhac/termglossary.pdf) on 6th December 2013 with its centre at 10°N and 84°E (Fig. 1). The system intensified further into a deep depression (DD) on the same day with maximum sustained wind speed of 50-60 km/hr. Subsequently, when it turned into a cyclonic storm (CS) on 7th December, the IMD named it as Madi. On further intensification into a severe cyclonic storm (SCS), the system started moving in a north/north-northeast direction with maximum sustained wind speed of 90-100 km/hr. Subsequently, on 8th December, the system turned into a very severe cyclone (VSCS) with maximum sustained wind speed of 120-130 km/hr. The system moved further northward on 9th December reaching the location 14.6°N and 84.7°E, when it weakened into SCS with maximum sustained wind speed of 110-120 km/hr. The system not only weakened but slowed down considerably while reaching the location 15.7°N and 85.3°E on 10th December where it remained stationary for a while. At that point the SCS deviated from its northward track, took a near 180 degree turn and veered southwestward (Fig. 1). During the course of its south-westward movement, the SCS weakened to CS with maximum sustained wind speed of 80-90 km/hr. On its further south-westward journey, the CS weakened to DD on 11th December and further to a depression the same day with its centre at 12.9°N and 82.7°E. On 12th December 2013 the depression further weakened to a well marked low pressure.

3 Results and Discussion

We start our analysis by examining the time-evolution of the spatial distribution of various oceanic and atmospheric parameters from 4th to 15th December 2013 to understand the thermo-dynamical and dynamical conditions that led to the formation and subsequent dissipation of cyclone Madi.

3.1 Thermodynamic conditions before, during and after the cyclone

Ocean heat content (OHC) plays an important role in the translation speed and intensification of cyclones over the BoB (Sadhuram et al., 2010). The time-evolution of the spatial distribution of the OHC on 4th December 2013 showed large values ranging from 3.580 to 3.600 x 10^{11} J/m^2, except a meridionally-elongated region along the western boundary between 8° and 20°N, and another small patch in the central BoB centered at 13°N, where the values were small (Fig. 2a, 2b). Note the meridional band of the large OHC, adjacent to the meridional band of small OHC hugging the western boundary, with three distinct patches of high values within them. The drastic decrease of OHC on 7th December (Fig. 2c, 2d) indicated strong heat uptake by the cyclonic storm during the process of its intensification. As the system moves northward, passing over the region of high OHC it continues to take up heat from the upper ocean and intensifies further (Fig. 2e). Note that on 9th December when the track of the system passes over a region of low OHC it weakens (Fig. 2f). On 10th December, when the system it deviated from its northward track and took almost a 180-degree turn it was passing through low OHC (Fig.2g). On its southward journey, the system passes over regions of lower OHC on 11th and 12th (Fig. 2h, 2i), when it dissipates into DD and to well-marked low pressure respectively. Once the system is dissipated, the spatial distribution of OHC showed a recovery in terms of heat gain by the upper ocean (Fig. 2j-l), especially in the region of the track of the cyclone.

3.2 Dynamic conditions before, during and after the cyclone

The analysis of the time-evolution of the spatial distribution of sea level anomaly (SLA) over-laid with geostrophic current from 4th to 15th December revealed the presence of several meso-scale cyclonic (blue region with negative SLA) and anticyclonic (red regions with positive SLA) eddies (Fig. 3). The SLA and associated geostrophic current clearly indicated the presence of two cyclonic eddies along the western boundary and two in the offshore region (Fig. 3a, b). The region of occurrence of these cyclonic eddies coincided with the region of low OHC (Fig. 2). Note that the genesis of Madi in the form of a depression occurred on 6th December in the region of positive SLA with an anticyclonic circulation (Fig. 3c), which was the same region that had high

OHC. The intensification of Madi on 8th December also occurred in a region of positive SLA with an anticyclonic circulation (Fig. 3d, 3e). On 9th December when the system entered into a region of negative SLA with cyclonic circulation (Fig. 4f), which was also a region of low OHC it weakened as it was deprived of the thermal energy from the upper warm ocean that is essential to sustain the system. On 10th December when the system moved further north entering towards the core of the cyclonic eddy (Fig. 3g) with low OHC (Fig. 2g) its further northward movement was arrested. It remained stationary for a while and changed its track to almost 180-degree in a southwestward direction. While doing so the cyclone Madi was moving further through the regions of strong cyclonic circulation/eddies (Fig. 3i), which rapidly reduced its strength and finally led to its dissipation on 12th December. The passage of cyclone Madi modified the upper ocean circulation in the southwestern part of the BoB (Fig. 3j-l) into a large cyclonic gyre with strong southward western boundary current from 17° to 10°N along the west coast of India. The four cyclonic eddies were now prominently seen embedded in this large-scale gyre.

When a cyclone passes over the cyclonic eddy region, the colder temperature within the eddy could potentially reduce the translation speed of the cyclone as well as its intensity as it is unable to fuel the cyclone as effectively as in the case of the warm water region where it originates. In order to further ascertain the role of cyclonic eddy in weakening the strength of the cyclone before its track reversal, we calculated the translational speed of the system from its formation on 6th to its dissipation on 12th December and examined it along with its strength (Table 1). It is clear from Table 1 that on 9th December when the cyclone entered the region of oceanic cyclonic eddy the translational speed of the cyclone decreased from 2.81 m/s to 1.96 m/s and the cyclone weakened from VSCS to SCS. Thereafter, subsequent to track reversal as the system moves south-westward out of the cyclonic eddy, the translation speed increases.

Though the weakening and the final dissipation of the cyclone Madi was easy to understand in the context of the prevailing oceanic cyclonic eddies, we examined the time-evolution of the spatial distribution of the atmospheric parameters such as wind at 850 hpa (Fig. 4), vertical wind shear between the 850 and 200 hPa (Fig. 5) and mid-troposheric (500hpa) relative humidity (Fig. 6) to understand the atmospheric condition.

The salient feature of the large-scale atmospheric circulation over the BoB, prior to the genesis of cyclone Madi, was the prevalence of an easterly zonal wind with speed between 5 and 15 m/s with an embedded cyclonic circulation located in the southwestern region (Fig. 4a, 4b). The wind speed associated with the cyclonic circulation was between 15 and 25 m/s. On 6th December when the depression was formed, this broad cyclonic circulation becomes well organized with a small central region having lower wind speeds of 10 m/s, while the surrounding regions had higher wind speeds of 20-25 m/s (Fig. 4c). When the system developed into the CS (Fig. 4d) and intensified into a VSCS (Fig. 4e), the large-scale atmospheric circulation in the BoB showed a well defined "eye of the cyclone". Away from the cyclonic circulation, the winds in the northen part of the BoB were mostly southwestward. On 9th December the weakening of the system was discernible as it moved northward (Fig. 4f). At this time the low vertical wind shear (10 to 15 m/s) (Fig. 5f) and high relative humidity (60-80 %) (Fig. 6f) were congenial for the system for further intensification or at least to sustain its intensity. In contrast the system weakened from VSCS to SCS. This indicated that the system evolution at this time was controlled by the oceanic cyclonic eddies rather than the atmospheric conditions. On 10th when the system reached its northern most location (Fig. 4g), it was actually sitting right on the top of the cold-core of the cyclonic eddy (Fig. 3g). At this time the system became stationary and the prevailing easterly winds (Fig. 4g) were able to turn and move it towards southwesterly direction, a result which is consistent with that of (Bhattacharya et al., 2015).

Thus, our study showed that the weakening of cyclone on its northward journey was mediated by the oceanic cold-core cyclonic eddy while the change in the direction of the cyclone track when the system was stationary was brought about by the prevailing northeasterly winds.

3.3 Cyclone-induced along track oceanic variability

In order to quantify the upper ocean response of the tropical cyclone Madi, we examined four oceanic parameters viz. SST, Ekman pumping velocity (EKV), SLA and OHC during the period 2 to 15 December 2013 at four locations : (1) Box A, the region of genesis of the depression which subsequently turned into cyclone Madi, (2) along Track 1, the northward path followed by the cyclone Madi during which time it intensified from CS to VSCS, (3) Box B, the region where the cyclone Madi weakened, remained stationary and eventually turned, and (4) along Track 2, the southwestward path of the cyclone which eventually dissipated.

The time-evolution of SST in Box A, showed a monotonic decline of 1.5^{o}C from 28.2^{o}C to 26.7^{o}C during the period from the genesis of the cyclone to its decay (Fig. 7). However, the rate of decrease during the entire period was not uniform. Even before the formation of the depression SST showed a weak decrease of 0.3^{o}C, however, during the period 6th to 8th December when the depression was formed within the Box A and turned into a cyclone, the SST decreased rapidly. Though the system was away from the region of Box A and was dissipating with time during 9th to 11th December, the SST within the Box A showed the most rapid decrease of 1.1^{o}C. The SLA, on the other hand, showed a continuous decrease, before the formation of depression and much after its dissipation. The SST showed a recovery/warming trend after 12th December. The EKV showed a peak on 6th December, at the time of formation of depression. This is expected, as under the action of cyclonic wind, the upward Ekman pumping will also increase in magnitude. What was unexpected was the temporal response of the OHC, which showed an initial decrease from 2nd to 3rd December followed by an increase reaching the highest value of 3.589 x 10^{11} J/m^2 and a subsequent decrease. A secondary peak occurred on 6th as the depression formed in the area of Box A. During 6th to 8th December when the system intensified and was located within the Box A, the OHC showed rapid decrease to a value of 3.574 x 10^{11} J/m^2. There after the values were closer to 3.576 x 10^{11} J/m^2, except on 13th December when it once again peaked to 3.578 x 10^{11} J/m^2.

Though the response of all the four parameters along Track 1 (Fig. 8), Track 2 (Fig. 9) and at Box B (Fig. 10) were similar to that of Box A (Fig. 7), a closer similarity was noticed between Box A and Track 2, and between Track 1 and Box B. However, the magnitudes of response of each parameter and their times of occurrence were different depending on the position of the cyclone with respect to each of the four locations. For example, the OHC showed an inverse relationship with the Ekman pumping velocity along Track 1(Fig. 8) and at Box B (Fig. 9), while at Box A (Fig. 7) and along Track 2 (Fig. 8) the OHC showed a double-peak structure. Along Track 1, the occurrence of highest value of EKV was consistent with the system intensifying into VSCS with a maximum sustained wind speed of 110-120 km/hr. Similarly, at Box B also the occurrence of the highest EKV coincided

Ocean Sci. Discuss., https://doi.org/10.5194/os-2018-133
Manuscript under review for journal Ocean Sci.
Discussion started: 28 January 2019

with the arrival of the cyclone at this location. The rapid decrease in SST occurred in all the four regions, in general, during 9th to 11th December, indicating a time-lag between the presence of the cyclonic storm and the peak of the upward EKV. Another noteworthy feature, common in all the four cases, was the co-variation of SST and SLA, both showing a monotonic decline, indicating the occurrence of colder waters associated with decreasing sea level, except along Track 2 (Fig. 9). Note that this lowered sea level and colder SST occurred well before the initiation of the upward Ekman pumping under the influence of the cyclone Madi. This pointed towards the pre-cyclone cooling of SST by oceanic cyclonic eddies, which was also evident from the time evolution of the spatial maps of daily SLA (Fig. 3). However, along Track 2, SLA showed a rapid increase from 2nd to 5thDecember followed by a slower increase until 8th December, well before the passage of the cyclone through this region. This is primarily due to the fact that the location of Track 2 passes through an anticyclonic eddy.

3.4 Depth-dependent temperature and chlorophyll *a* response

Having analyzed the cyclone-induced SST response along the track of the cyclone, it is pertinent to examine the vertical profiles of temperature before, during and after the passage of cyclone Madi. Hence, we examined the vertical profiles of temperature in the vicinity of Track 2 obtained by two Argo floats (ID-2901288 and ID-2901629) which transected the northern and southern parts of Track 2 during the period of study (see Fig. 1 for the location of Argo floats). The vertical profiles of temperature obtained from both the Argo floats (Fig. 11a, b) showed the presence of a thermal inversion (0.2 to 0.3^{o}C) located in the upper 40 m prior to the passage of the cyclone Madi, which disappears in the subsequent profiles. The most distinct change was in the mixed layer temperature and depth. On 4th December prior to the formation of cyclone the mixed layer depth (MLD) obtained from Argo float with ID-2901288 was 30m and temperature was 28.2^{o}C and after the passage of cyclone on 14th December the MLD was 50 m and temperature was 26.5^{o}C (Fig. 11a). A similar change was also noticed in the vertical profiles of temperature obtained from Argo float with ID-2901629 (Fig. 11b). Thus, both the Argo floats captured the cyclone-induced mixed layer cooling and deepening.

The vertical profiles of Chl-*a* obtained from the Bio-Argo float (ID-2902086) showed low values prior to the cyclone (23rd November to 3rd December 2013) in the range of 0.10 to 0.15 mg/m^3 with constant value within the mixed layer and a subsurface chlorophyll maximum (SCM) located at about 50m (Fig. 11c). The vertical profiles of Chl-*a* showed a progressive increase during and after the cyclone in both the surface as well as the subsurface values reaching a maximum of 0.45 and 0.65 mg/m^3 respectively on 23rd December 2013. Thereafter, it showed a decline on 28th December 2013 when the value in the upper 60 m was 0.40 mg/m^3 with no perceptible SCM. Thus, the Chl-*a* profiles in the upper 60 m showed maximum impact due to the cyclone leading to an overall increase in the biomass.

3.5 Cyclone-induced biogeochemical variability

It is well known that tropical cyclones bring about large changes in the upper ocean productivity as well as gas-exchange between ocean and atmosphere. In order to understand and quantify the biogeochemical response due to the cyclone Madi, we examined along track variation of satellite-derived chlorophyll *a* pigment concentration (Chl-*a*), net primary production (NPP), and the net CO_2 flux. A major difficulty with the remotely sensed Chl-*a* pigment concentration is the lack of adequate cloud-free pixels along track on a daily time scale. In order to overcome this, we have used weekly composite data for Chl-*a* for the calculation of NPP from 30th November to 28th December in the four regions, viz. Box A and B and Track 1 and 2 (Fig. 1), while the net CO_2 flux was computed on daily time scale from 2nd to 15th December 2013.

The time variation of the weekly composite of Chl-*a* showed a pattern that was typical of the cyclone induced response (Fig. 12). Prior to the genesis of cyclone Madi, the Chl-*a* was in the range of 0.2 to 0.4 mg/m^3, but the weekly composite values for the period 7th to 14th December, which includes the growth, decay and a couple of days after cyclone, showed several fold increase. The maximum increase of 2.7 mg/m^3 was in Box B, which was almost 7-times higher than the pre-cyclone period. The minimum increase of 1 mg/m^3 occurred along the Track 2, which was 5-times higher than the pre-cyclone period. In the Box A and along Track 1, the Chl-*a* values were 1.4 and 1.5 mg/m^3 respectively after the cyclone. It is pertinent to examine the chlorophyll enhancement by other cyclones in the BoB and compare with the present study. For example, the Orissa super cyclone in October 1999 produced a Chl-*a* enhancement in the rage of 0.38 to 0.97 mg/m^3 in the open ocean region (Madhu et al., 2002), while that near the land fall region was a maximum of 1.0 mg/m^3 (Patra et al., 2007). (Vinayachandran et al., 2003) reported a value ranging from 0.5 to 2.0 mg/m^3 for the cyclones that occurred during November-December during the period 1996 to 2001. In the case of cyclone Sidr in 2007, (Maneesha et al., 2011) obtained an increase from 0.2 to 0.5 mg/m^3.

Thus, the Chl-*a* enhancement by Madi was much greater than for previous cyclones that occurred in the BoB. The obvious question would be why the Chl-*a* along both the tracks as well as the boxes showed an increase and why Box B showed the highest magnitude of Chl-*a* response to the cyclone. Recall that the EKV showed a rapid increase during the period when the cyclone was transiting these regions, while a concomitant rapid decrease of SST was also noticed. This indicated the upward transport of cold subsurface waters under the influence of the cyclonic winds. As the subsurface waters are nutrient rich, the increased Ekman pumping under the tropical cyclone would bring more nutrients to the upper oceans which will kick-start the photosynthesis (Subrahmanyam et al., 2002; Lin et al., 2003) resulting in the observed increase in the Chl-*a* biomass. Recall also that an oceanic cyclonic eddy was located in the region of Box B where the cyclone was stationary for a while. In the BoB, the nutricline is located just below the mixed layer, usually at a depth ranging from 20 to 40m (Prasanna Kumar et al., 2007), and the eddy-pumping (Falkowski et al., 1991) associated with oceanic cyclonic eddies is able to supply sub-surface nutrients to the surface waters (Prasanna Kumar et al., 2004). Hence, we infer that under the combined effect of the oceanic eddy and the cyclone Madi, the upward Ekman pumping would have been stronger and more nutrients could be supplied to the upper ocean, which resulted in the observed 7-fold increase. The lowest response, 5-fold increase, was seen along track 2, which is to be expected as when the cyclone transited along this path it was decaying rapidly. Note that by the last week of

December (21-28) the Chl-*a* values came back to their pre-cyclone values. Thus, in response to the cyclone Madi, the Chl-*a* in all the 4 regions, which were under its influence, exhibited enhancement, though to varying magnitudes. The increase in Chl-*a* concentration was rapid during the enhancement period, while the decline took more time.

Consistent with the Chl-*a* response, the NPP (Fig.13) showed a similar pattern of co-variability with highest value of 2500 mg C m^{-2} day^{-1} occurring in Box B, which was also 8-fold higher than the pre-cyclone value. Similarly, the least enhancement in NPP was shown along Track 2 with a value of 800 mg C m^{-2} day^{-1}, which was only 2-and-half fold increase from its pre-cyclone value. The enhancements along Track1 and at Box A were 5-fold and 2-fold respectively compared to pre-cyclone values. Being a weekly composite, in both Chl-*a* and NPP, it was not possible to resolve the exact date of enhancement or decline, though the overall pattern was discernible.

It has been shown by several studies that out-gassing of CO_2 from ocean to atmosphere takes place under the influence of tropical cyclones (see for e.g. Bates et. al., 1998; Nemeto et al., 2009). This happens in two ways – firstly, the strong wind associated with cyclones results in out-gassing from ocean to atmosphere; secondly, the supply of subsurface dissolved inorganic carbon to the surface due to the upward Ekman pumping by the wind stress curl and it's out-gassing due to heating and equilibration with the atmosphere. We examined the daily variation of total CO_2 flux in all the 4 regions from 2nd to 15th December 2013 (Fig. 14) to decipher this. All the four regions showed enhanced net CO_2 flux to the atmosphere, though the magnitude and timing were different. Again consistent with Chl-*a* and NPP, the maximum CO_2 out-gassing to the atmosphere was seen in Box B and the least was along Track 2. In Box B, the fastest CO_2 out-gassing of 4.7 Tg carbon per day to the atmosphere took place when the cyclone Madi was in this Box region and was 3.7-fold higher than its average pre-cyclone value. The maximum CO_2 out-gassing of 2.5 Tg carbon per day to the atmosphere took place along Track 2 and was 2-fold greater than its average pre-cyclone value. The maximum value of CO_2 out-gassing at Box A and along Track 1 was similar to that of Track 2. A secondary peak in CO_2 out-gassing was seen at Box B and along Track 2 on 11th December 2013, while Box A and Track 1 did not show such a pattern.

4. Summary and Concluding Remarks

The ocean-atmosphere conditions associated with category-2 tropical cyclone Madi in the southwestern BoB during 6th to 12th December 2013 were studied using a suite of in situ and remote sensing data sets. We infer that the origin of cyclone Madi and its and strengthening from CS to VSCS was facilitated by the large OHC. On its northward movement when it passed over an oceanic cold-core cyclonic eddy, the system weakened to SCS and its translation speed was decreased by almost 1 m/s. In spite of the prevailing favorable atmospheric conditions for the strengthening of a cyclone, such as low vertical wind shear and high relative humidity, the system did not strengthen further; instead it remained weak. At this stage the prevailing northeasterly winds altered the track of the weakened system by almost 180-degree. On its southward journey the system passed over cold-core eddies that rapidly dissipated it.

The cyclone Madi triggered intense physical and biogeochemical response in the upper ocean. The weekly composite of satellite-derived Chl-*a* pigment concentration showed an enhancement that ranged from 5 to 7-fold with a maximum value of 2.7 mg/m^3. A similar response was seen in the net primary productivity which showed a 2.5 to 8-fold increase, with a maximum value of 2500 mg C m^{-2} day^{-1}. The largest values of both Chl-*a* and NPP was greater than for previous cyclones in the BoB. Out study indicates that a combination of an oceanic cyclonic eddy along with cyclone Madi facilitated upward Ekman pumping of nutrient rich subsurface waters to the surface, thereby kick-starting the primary production and increasing the chlorophyll biomass. Consistent with this, the net CO_2 out-gassing to the atmosphere also was the greatest in this region amounting to 4.7 Tg carbon per day, which was 3.7-fold greater than the pre-cyclone values. Our study emphasizes the importance of eddy-cyclone interaction that led to the large increase in Chl-*a*, primary production and CO_2 out-gassing. Since cyclone and eddies co-occur in many parts of the world ocean our approach can be adopted in other regions to quantify the biogeochemical response.

One of the limitations of our study is the lack of modeling to quantify the eddy-cyclone interaction. Our study underscores the important role of oceanic eddies in understanding the life cycle of tropical cyclones in the BoB. Since both cyclonic and anticyclonic eddies are ubiquitous in the BoB, they will impact both the translation speed and intensity of a tropical cyclone. Hence, for the accurate prediction of a cyclone track and its intensity, there is an urgent need to incorporate eddies into the predictive models; this action is still to be explored. This will be attempted in the near future.

Author Contribution

S. Prasanna Kumar and Arun Chakraborty formulated the problem, and were involved continuously during the conduction of the work. Riyanka Roy Chowdhury has been the primary researcher and has carried out all the data analyses, computation and derivations, and preparation of the graphics required for the manuscript. S. Prasanna Kumar and Riyanka Roy Chowdhury were involved in the preparation of the manuscript.

Acknowledgements

The authors thank Directors of Indian Institute of Technology (IIT), Kharagpur and CSIR-National Institute of Oceanography (CSIR-NIO), Goa and the Council of Scientific and Industrial Research (CSIR), New Delhi for all the support and encouragement for this research. The daily SST data are available from (http://www.incois.gov.in/tropflux_datasets/ data/ daily/), daily SLA data along with zonal and meridional geostrophic velocity are from (https://www.aviso.altimetry.fr/en/my-aviso.html), surface wind data are from (https://opendap.jpl.nasa.gov/opendap/OceanWinds/ascat/preview/L2/metop_a/12km/contents.html), while the wind at 850 hpa is from(http://www.ncep.noaa.gov). The Argo data are from (http://www.coriolis.eu.org/Data-Products/Data-Delivery/Data-selection). The graphics were generated using MATLAB and the code used in this paper can be obtained from the first author. Riyanka Roy Chowdhury acknowledges Ministry of Human Resource Development for providing the research fellowship. NIO contribution number is XXXX.

References

Ali, M. M., Jagadeesh, P. S. V., Jain, S.: Effects of eddies on Bay of Bengal cyclone intensity, Eos Transactions American Geophysical Union, 88, 93-95, 2007.

Babin, S . M., Carton, J. A., Dickey, T.D., Wiggert, J. D.: Satellite evidence of hurricane-induced phytoplankton blooms in an oceanic desert, Journal of Geophysical Research, 109, C03043, https://doi.org/10.1029/2003JC001938, 2004.

Basu, B. K., Bhagyalakshmi K.: Forecast of the track and intensity of the tropical cyclone AILA over the Bay of Bengal by the global spectral atmospheric model VARSHA, Current Science, 99, 765-775, 2010.

Bates, N. R., Knap, A. H., Michaels, A. F.: Contribution of hurricanes to local and global estimates of air-sea exchange of CO_2, Nature, 395, 58-61, 1998.

Behrenfeld, M. J., Falkoswski, P.G.: Photosynthetic rates derived from satellite based chlorophyll concentration, Limnology and Oceanography, 42, 1-20, 1997.

Bentamy, A., Croize-Fillon, D.: Gridded surface wind fields from Metop/ASCAT measurements, International Journal of Remote Sensing, 33, 1729-1754, 2012.

Bhattacharya, S. K., Kotal, S. D., Kundu, P. K.: An Analysis of recurvature and decay of the tropical cyclone 'MADI' over the Bay of Bengal, Tropical Cyclone Research and Review, 4, 27-37, https://doi.org/10.6057/2015tcRR01.04, 2015.

Chang, S. W., Anthes, R. A.: The mutual response of the tropical cyclone and the ocean, Journal of Physical Oceanography., 9, 128-135, 1979.

Das, Y., Mohanty, U. C., Jain, I.: Development of tropical cyclone wind field for simulation of storm surge/sea surface height using numerical ocean model, Modeling Earth Systems and Environment, 2:13, https://doi.org/10.1007/s40808-015-0067-5, 2016.

Dube, S.K., Rao, A.D., Sinha, P.C., Murty, T.S., Bahuleyan, N.: Storm surge in Bay of Bengal and Arabian Sea: the problem and its prediction, Mausam, 48, 288-304, 1997.

Emanuel, K. A.: Thermodynamic control of hurricane intensity, Nature, 401, 665-669, 1999.

Falkowski, P. G., Ziemann, D., Kolber, Z.,Bienfang, P. K.: Role of eddy pumping in enhancing primary production in the ocean, Nature, 352, 55-58, 1991.

Geetha, G., UdayaBhaskar, T.V. S., Eluri, P. R.R.: Argo data and products of Indian ocean for low bandwidth users, Int. Journal of Ocean and Oceanography, 5, 1-8, 2011.

Gill, A. E.: Atmosphere-ocean dynamics, Academic Press, London, UK, 1982.

Jaimes, B., Shay, L.K.: Mixed layer cooling in mesoscale oceanic eddies during hurricanes Katrina and Rita, Monthly Weather Review, 137, 4188-4207. https://doi.org/10.1175/2009MWR2849.1, 2009.

Kalnay, E., Kanamitsu, M., Kistler, R., Collins, W., Deaven, D., Gandin, L., Iredell, M., Saha, S., White, G., Woollen, J., Zhu, Y., Chelliah, M., Ebisuzaki, W., Higgins, W., Janowiak, J., Mo, K. C., Ropelewski, C., Wang,

Ocean Sci. Discuss., https://doi.org/10.5194/os-2018-133
Manuscript under review for journal Ocean Sci.
Discussion started: 28 January 2019

J., Leetmaa, A., Reynolds, R., Jenne, R., Joseph , D.: The NCEP/NCAR 40-year reanalysis project, Bull. American Meteorological Society, 77, 437-470, 1996.

Kanase, D. R., Salvekar, P. S.: Study of weak intensity cyclones over Bay of Bengal using WRF model, Atmospheric and Climate Sciences, 4, 534-548, 2014.

Kotal, S. D., Bhattacharya, S. K., Roy Bhowmik, S. K., Kundu, P. K.: The rapid growth and decay of severe cyclone JAL over the Bay of Bengal, Meteo. and Atmos. Phy, 121, 161- 179, 2013.

Lin, I.-I., Wu,C.-C., Emanuel, K. A., Lee, I.-H., Wu,C.-R.,Pun,I.-F.: The interaction of Supertyphoon Maemi (2003) with a warm ocean eddy, Monthly Weather Review, 133, 2635–2649, 2005.

Lin, I. -I., Liu, W. T., Wong, C.-C., Wong, G. T. F., Hu, C., Chen, Z., Liang, W.-D., Yang, Y., Liu, K.-K.: New evidence for enhanced ocean primary production triggered by tropical cyclone, Geophysical Research Letters, 30, 1718, https://doi.org/10.1029/2003GL017141 , 2003.

Lin, I. -I., Chen, C. H., Pun, I. F., Liu, W. T., Wu, C. -C.: Warm ocean anomaly, air sea fluxes, and the rapid intensification of tropical cyclone Nargis, Geophysical Research Letters, 36, 3817, https://doi.org/10.1029/2008GL035815, 2009.

Lin, I. -I., Chou, M. D., Wu, C. -C.: The impact of a warm ocean eddy on Typhoon Morakot 2009: A preliminary study from satellite observations and numerical modeling, Terrestrial Atmospheric and Oceanic Sciences , 22, 661-671, 2011.

Liu, X., Wang, M., Shi, W.: A study of a hurricane Katrina-induced phytoplankton bloom using satellite observations and model simulations, Journal of Geophysical Research, 114, C03023, https://doi.org/10.1029/2008JC004934, 2009.

Ma, Z., Fei, J., Liu, L., Huang, X., Cheng, X.: Effects of the cold core eddy on tropical cyclone intensity and structure under idealized air-sea interaction conditions, Monthly Weather Review, 141, 1285-1303, 2013.

Madhu, N. V., Maheswaran, P.A., Jyothibabu, R., Revichandran, C., Balasubramanian, T., Gopalakrishna, T. C., Nair, K.K.C.: Enhanced biological production off Chennai triggered by October 1999 super cyclone (Orissa), Current Science, 82, 1472-1479, 2002.

Maneesha, K., Sarma, V.V.S.S., Reddy, N. P. C., Sadhuram, Y., RamanaMurty, T. V., Sarma, V. V., Dileep, K. M.: Meso-scale atmospheric events promote phytoplankton blooms in the coastal Bay of Bengal, Journal of Earth System Science, 120, 773-782, 2011.

Mathew, S., Natesan, U., Latha, G., Venkatesan, R., Rao, R. R., Ravichandran, M.: Observed warming of sea surface temperature in response to tropical cyclone thane in the Bay of Bengal, Current Science, 114, 1407-1413, 2018.

McPhaden, M. J., Foltz, G. R., Lee, T., Murty, V. S. N.,Ravichandran, M., Vecchi, G., Vialard, J., Wiggert, J. D., Lisan, Y.: Ocean-atmosphere interactions during cyclone Nargis, Eos Transactions American Geophysical Union, 90, 53-54, 2009.

Narvekar, J., Prasanna Kumar, S., 2006. Seasonal variability of the mixed layer in the central Bay of Bengal and associated changes in nutrients and chlorophyll, Deep-Sea Research I, 53, 820-835, 2006.

Narvekar, J., Prasanna Kumar, S.: Mixed layer variability and chlorophyll a biomass in the Bay of Bengal, Biogeosciences, 11, 3819-3843, 2014.

Nemoto, K., Midorikawa, T., Ogawa, A., Takatani, S., Kimoto, H., Ishii, M., Inoue, H.Y.: Continuous observations of atmospheric and oceanic CO_2 using a moored buoy in the East China Sea: Variations during the passage of typhoons, Deep-Sea Research II, 56, 542-553, 2009.

O'Brien, J. J., Reid, R. O.: Thenon-linear response of a two layer baroclinic ocean to a stationary, Axially-symmetric Hurricane: Part-I. upwelling induced by momentum transfer, Journal of Atmospheric Science, 24, 197-207, 1967.

Patnaik, K.V.K.R.K., Maneesha, K., Sadhuram, Y., Prasad, K.V.S.R., RamanaMurty, T.V., Bramhananda Rao, V.: East India coastal current induced eddies and their interaction with tropical storms over Bay of Bengal, Journal of Operational Oceanography, 7, 58-68, 2014.

Patra, P. K., Kumar, M. D., Mahowald, N., Sarma, V.V.S.S.: Atmospheric deposition and surface stratification as controls of contrasting chrolophyll abundance in the North Indian Ocean, Journal of Geophysical Research, 112, C05029, 2007.

Prakash, K. R., Pant, V.: Upper oceanic response to tropical cyclone Phailin in the Bay of Bengal using a coupled atmosphere-ocean model, Ocean Dynamics, 67, 51-64, 2017.

Prasanna Kumar, S., Nuncio, M., Narvekar, J., Kumar, A., Sardesai, S., Desouza, S. N., Gauns, M.,Ramaiah, N., Madhupratap, M.: Are Eddies nature's trigger to enhance biological productivity in the Bay of Bengal?, Geophysical Research Letters, 31, L07309, 2004.

Prasanna Kumar, S., Nuncio, M., Ramaiah, N., Sardesai, S., Narvekar, J., Veronica F., Paul, J.T.: Eddy-mediated biological productivity in the Bay of Bengal during fall and spring intermonsoons, Deep Sea Research I, 54, 1619–1640, 2007.

Praveen Kumar, B., Vialard,J., Legaigne,M., Murty, V.S.N., McPhaden, M.J.: TropFlux: air-sea fluxes for the global tropical oceans-description and evaluation, Climate Dynamics, 38, 1521-1543, 2012.

Premkumar, K., Ravichandran, M., Kalsi, S. R., Sengupta, D., Gadgil, S.: First results from a new observational system over the Indian Seas, Current Science, 78, 323-330, 2000.

Price, J. F.: Upper ocean response to a hurricane, Journal of Physical Oceanography, 11, 153-175, 1981.

Pun, I.F., Chang, Y.-T., Lin, I.-I., Tang, T.Y., Lien. R.-C.: Typhoon-ocean interaction in the western North Pacific. Part 2, Oceanography, 24, 32–41, 2011.

Rao, K. H., Smitha, A., Ali, M. M.: A study on cyclone induced productivity in southwestern Bay of Bengal during November-December 2000 by MODIS (SST and Chlorophyll-a) and altimetry sea surface height observation, Indian Journal of Marine Sciences, 35, 153–160, 2006.

Rao, A. D., Dash, S., Babu, S. V., Jain, I.:, Numerical modeling of cyclone impact on the ocean-a case study of the Orissa Supper Cyclone, Journal of Coastal Research, 23, 1245–1250, 2007.

Reynolds, R. W., Smith, T. M., Liu, C., Chelton, D. B., Casey, K. S., Schlax, M. G.: Daily high-resolution blended analyses for sea surface temperature, Journal of Climate, 20, 5473-5496, 2007.

Sadhuram, Y.: Record decrease of sea surface temperature following the passage of a super cyclone over the Bay of Bengal, Current Science, 86, 383-384, 2004.

Sadhuram, Y., Maneesha, K., RamanaMurty, T. V.: Importance of upper ocean heat content in the intensification and translation speed of cyclones over the Bay of Bengal, Current Science, 99, 1191-1193, 2010.

Sadhuram, Y., Maneesha, K., RamanaMurty, T. V.: Intensification of Aila due to a warm core eddy in the north Bay of Bengal, Natural Hazards, 63, 1515-1525, 2012.

Saha, S., Moorthi, S., Wu, X., Wang, J., Nadiga, S., Tripp, P., Behringer, D., Hou,Y-T., Chuang, H-Y., Iredell, M., Ek, M., Meng, J., Yang, R., Mendez, M.P., Dool, H V D., Zhang, Q., Wang, W., Chen, M., Beeker, E.: The NCEP Climate Forecast System Version 2, Journal of Climate, 27, 2185–2208, 2014.

Sarangi, R. K.: Impact of cyclones on the Bay of Bengal chlorophyll variability using remote sensing satellites, Indian Journal of Geo-Marine Sciences, 40, 749-801, 2011.

Sengupta, D., Bharath, R. J., Anitha, D. S.: Cyclone-induced mixing does not cool SST in the post-monsoon north Bay of Bengal, Atmospheric Science Letters, 9, 1-6, 2008.

Shay, L.K., Goni, G.J., Black, P.G.: Effect of a warm oceanic feature on hurricane Opal, Monthly Weather Review, 128, 1366-1383, 2000.

Srinivas, C. V., Yesubabu, V., Hriprasad, K.B.R.R., Ramakrishna, S. S. V. Venkatraman, B.: Real-time prediction of a severe cyclone 'Jal ' over Bay of Bengal using a high resolution mesoscale model WRF (ARW), Natural Hazards, 65, 331-357, 2013.

Subrahmanyam, B., Rao, K. H., Rao, N. S., Murty, V. S. N.: Influence of a tropical cyclone on chlorophyll a concentration in the Arabian Sea, Geophysical Research Letters, 29, 2065, https://doi.org/10.1029/2002GL015892, 2002.

Subrahmanyam, B., Murty, V.S.N., Sharp, R. J., O'Brien, J. J.: Air–sea coupling during the Tropical Cyclones in the Indian Ocean: a case study using satellite observations, Pure and Applied Geophysics, 162, 1643–1672, 2005.

Sun, L., Li, Y.-X., Yang, Y.-J., Wu, Q., Chen, X.-T., Li, Q.-Y., Li, Y.-B., Xian, T.: Effects of super typhoons on cyclonic ocean eddies in the western North Pacific: A satellite data-based evaluation between 2000 and 2008, Journal of Geophysical Research: Oceans, 119, 5585–5598, 2014.

Takahashi, T., Sutherland, S.C., Wanninkhof, R., Sweeney, C., Feely, R. A., Chipman, D.W., Hales, B., Friederich, G., Chavez, F., Sabine, C., Watson, A., Bakker, D.C.E., Schuster, U., Metzl, N., Yoshikawa-Inoue, H., Ishii, M., Midorikawa, T., Nojiri, Y., Körtzinger, A., Steinhoff, T., Hoppema, M., Olafsson, J., Arnarson, T.S., Tilbrook, B., Johannessen, T., Olsen, A., Bellerby, R., Wong, C.S., Delille, B., Bates, N.R., de Baar, J.W.H., 2009. Climatological mean and decadal changes in surface ocean pCO_2, and net sea-air CO_2 flux over the global oceans, Deep-Sea Research II, 56, 554-577, 2009.

Thomas, A., Samala, B.K., Kaginalkar, A.: Simulation of north Indian Ocean tropical cyclone using RAMS numerical weather prediction model, Tropical Cyclone Research and Review, 3, 1-9, 2014.

Tripathy, M., Raman, M., Dwivedi, R., Ajai, A.: Frequency of cyclonic disturbances and changing productivity patterns in the North Indian Ocean region: A Study Using Sea Surface Temperature and Ocean Colour Data, International Journal of Geosciences, 3, 490-506, 2012.

Tummala, S. K., Mupparthy, R. S., Kumar, M. N., Nayak, S. R.: Phytoplankton bloom due to cyclone Sidr in the central Bay of Bengal, Journal of Applied Remote Sensing, 3,033547, https://doi.org/10.1117/1.3238329, 2009.

Vidya, P. J., Das, S., Mani Murali, R.: Contrasting Chl-a responses to the tropical cyclones Thane and Phailin in the Bay of Bengal, Journal of Marine Systems, 165, 103-114, 2017.

Vinayachandran, P. N., Mathew, S.: Phytoplanktom bloom in the Bay of Bengal during the north east monsoon and its intensification by cyclones, Geophysical Research Letters, 30, 1572, 2003.

Vissa, N. K., Satyanarayana, A. N. V., Prasad, K. B.: Response of upper ocean and impact of barrier layer on Sidr cyclone induced sea surface cooling, Ocean Science Journal, 48, 279-288, 2013.

Wada, A., Chan, J.C.L.: Relationship between typhoon activity and upper ocean heat content, Geophysical Research Letters, 35, L17603, https://doi.org/10.1029/2008GL035129, 2008.

Wanninkhof, R.: Relationship between wind speed and gas exchange over the ocean, Journal of Geophysical Research, 97, 7373-7382, 1992.

Weiss, R. F.: Carbon dioxide in water and seawater: the solubility of a non-ideal gas, Marine Chemistry, 2, 203-215, 1974.

Yablonsky, R. M., Ginis, I.: Impact of a warm ocean eddy's circulation on hurricane-induced sea surface cooling with implication for hurricane intensity, Monthly Weather Review, 141, 997–1021, 2013.

Ocean Sci. Discuss., https://doi.org/10.5194/os-2018-133
Manuscript under review for journal Ocean Sci.
Discussion started: 28 January 2019

Table 1 Translation speed of the cyclonic disturbance along with its category during the life cycle of cyclone Madi. L-low pressure, DD-deep depression, CS-cyclonic storm, SCS-severe cyclonic storm, VSCS-very severe cyclonic storm.

Date	**Translation Speed (m/s)**	**Category of Cyclonic Disturbance**
06/12/2013	1.63	DD
07/12/2013	2.48	CS to SCS
08/12/2013	2.81	VSCS
09/12/2013	1.96	SCS
10/12/2013	2.32	CS
11/12/2013	3.44	DD
12/12/2013	5.41	L

Ocean Sci. Discuss., https://doi.org/10.5194/os-2018-133
Manuscript under review for journal Ocean Sci.
Discussion started: 28 January 2019

Figure Captions

Figure 1 Map showing the track of the tropical cyclone Madi (magenta filled circles inside the black circles) during 6-12 December 2013 in the Bay of Bengal obtained from UNISYS Weather. The shading is the sea level anomaly (m), while vectors are the wind (m/s) at 850 hpa, both are composite for the period 6-12 December 2013. Location of Box A, Track 1, Box B, Track 2, rectangular Box abcd, and Argo floats (ID-2901288 red plus & ID-2901629 yellow plus) near Track 2 are also shown in the map. The black hollow circles (seen as dark circles due to overlap) show the position of Bio-Argo float (ID2902086).

Figure 2 Spatial maps of oceanic heat content (x10^{11} J/m^2) from 4th (a) to 15th (l) December 2013 with track of the cyclone overlaid. The black filled circles represent the position of the cyclone on a particular day, while the magenta filled circles indicate the track.

Figure 3 Spatial maps of sea level anomaly (m) from 4th (a) to 15th (l) December 2013 with track of the cyclone overlaid. The black filled circles represent the position of the cyclone on a particular day, while the magenta filled circles indicate the track.

Figure 4 Spatial maps of wind speed (shading, m/s) overlaid with wind vectors (thin arrow) at 850 hpa from 4th (a) to 15th (l) December 2013 with track of the cyclone overlaid. The black filled circles represent the position of the cyclone on a particular day, while the magenta filled circles indicate the track.

Figure 5 Spatial maps of vertical wind velocity difference between the 850 and 200hPa (shading, m/s) from 4th (a) to 15th (l) December 2013 with track of the cyclone overlaid. The black filled circles represent the position of the cyclone on a particular day, while the magenta filled circles indicate the track.

Figure 6 Spatial maps of relative humidity (%) overlaid with winds at mid-troposhere (500hpa) from 4th (a) to 15th (l) December 2013 with track of the cyclone overlaid. The black filled circles represent the position of the cyclone on a particular day, while the magenta filled circles indicate the track.

Figure 7 Space-averaged variation of the sea surface temperature (SST, ^{o}C), Ekman pumping velocity (EKV, m/day, positive upward), oceanic heat content (OHC, x 10^{11} J/m^2) and sea level anomaly (SLA, m) in Box A from 2-15 December 2013.

Figure 8 Along track variation of the sea surface temperature (SST, ^{o}C), Ekman pumping velocity (EKV, m/day, positive upward), oceanic heat content (OHC, x 10^{11} J/m^2) and sea level anomaly (SLA, m) along Track 1 from 2-15 December 2013. These are daily averages along the track.

Figure 9 Space-averaged variation of the sea surface temperature (SST, ^{o}C), Ekman pumping velocity (EKV, m/day, positive upward), oceanic heat content (OHC, x 10^{11} J/m^2) and sea level anomaly (SLA, m) in Box B from 2-15 December 2013.

Figure 10 Along track variation of the sea surface temperature (SST, ^{o}C), Ekman pumping velocity (EKV, m/day, positive upward), oceanic heat content (OHC, x 10^{11} J/m^2) and sea level anomaly (SLA, m) along Track 2 from 2-15 December 2013. These are daily averages along the track.

Figure 11 Time-series of the vertical profiles of temperature (^{o}C) in the vicinity of Track 2 obtained from (a) Argo float ID-2901288 for 4, 9, 14, 19 and 24 December 2013, (b) Argo float ID-2901629 for 2, 12 and 22 December 2013 and (c) chlorophyll *a* (mg/m^3) in the vicinity of Track 1 obtained from Bio-Argo ID-2902086 for 23 and 28 November and 3, 8, 13, 18, 23 and 28 December 2013.

Figure 12 Time variation of weekly composite of chlorophyll *a* pigment concentrations (Chl-*a*, mg/m^3) in the Box A (red) and B (blue) and along Track 1 (green) and 2 (black) from 30 November to 28 December 2013. The vertical lines are the standard deviations.

Figure 13 Time variation of weekly composite of net primary production (NPP, mg C m^{-2} day^{-1}) in the Box A (red) and B (blue) and along Track 1 (green) and 2 (black) from 30 November to 28 December 2013. The vertical lines are the standard deviations.

Figure 14 Daily variation total CO2 flux (terra gram carbon per day) in the Box A (red) and B (blue) and along Track 1 (green) and 2 (black) from 2 to 15 December 2013. The vertical lines are the standard deviations.

Ocean Sci. Discuss., https://doi.org/10.5194/os-2018-133
Manuscript under review for journal Ocean Sci.
Discussion started: 28 January 2019

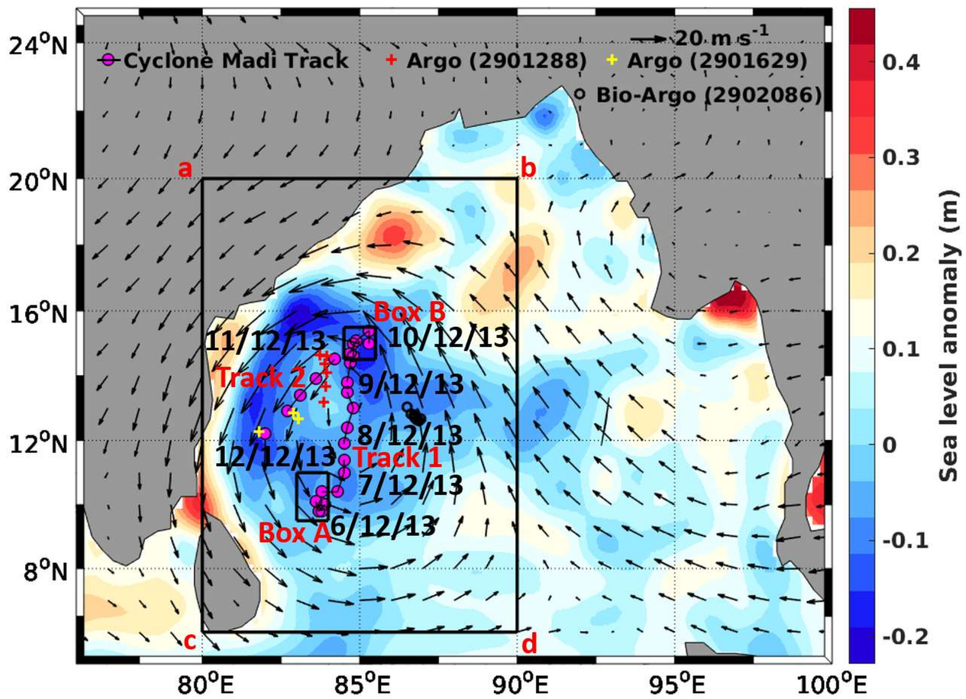

Figure 1 Map showing the track of the tropical cyclone Madi (magenta filled circles inside the black circles) during 6-12 December 2013 in the Bay of Bengal obtained from UNISYS Weather. The shading is the sea level anomaly (m), while vectors are the wind (m/s) at 850 hpa, both are composite for the period 6-12 December 2013. Location of Box A, Track 1, Box B, Track 2, rectangular Box abcd, and Argo floats (ID-2901288 red plus & ID-2901629 yellow plus) near Track 2 are also shown in the map. The black hollow circles (seen as dark circle due to overlap) show the position of Bio-Argo float (ID2902086).

Ocean Sci. Discuss., https://doi.org/10.5194/os-2018-133
Manuscript under review for journal Ocean Sci.
Discussion started: 28 January 2019

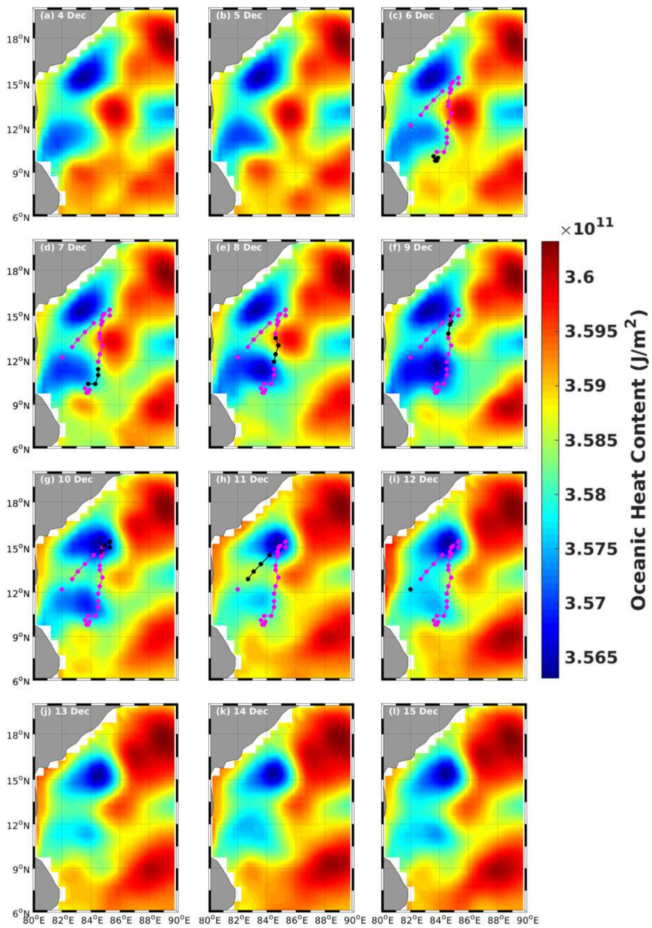

Figure 2 Spatial maps of oceanic heat content (x10^{11} J/m^2) from 4th (a) to 15th (l) December 2013 with track of the cyclone overlaid. The black filled circles represent the position of the cyclone on a particular day, while the magenta filled circles indicate the track.

Ocean Sci. Discuss., https://doi.org/10.5194/os-2018-133
Manuscript under review for journal Ocean Sci.
Discussion started: 28 January 2019

Ocean Science
Discussions
Open Access

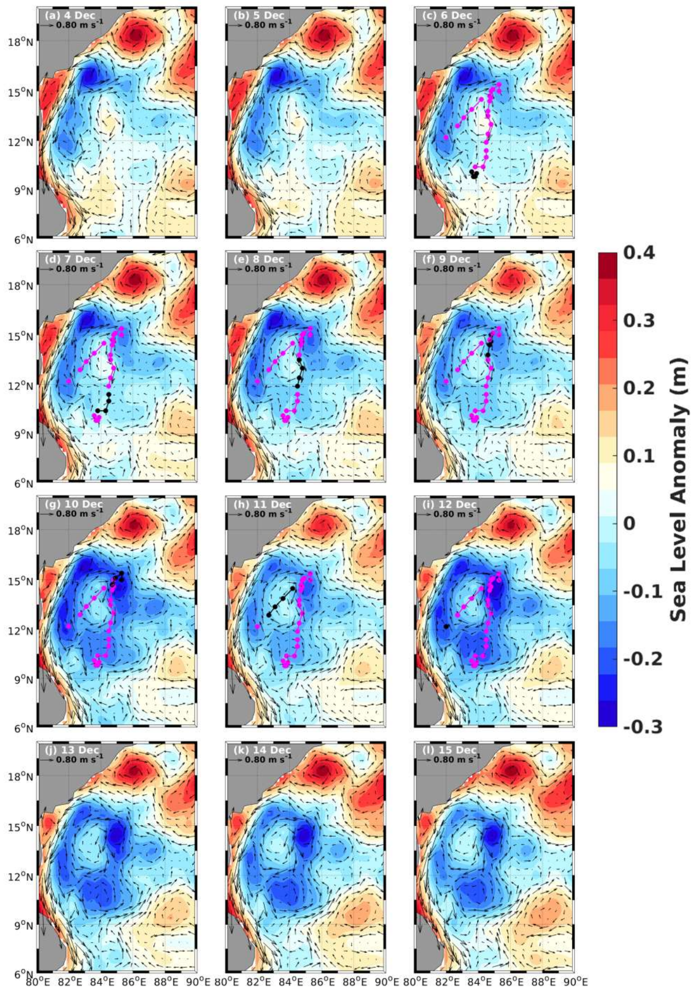

Figure 3 Spatial maps of sea level anomaly (m) from 4th (a) to 15th (l) December 2013 with track of the cyclone overlaid. The black filled circles represent the position of the cyclone on a particular day, while the magenta filled circles indicate the track.

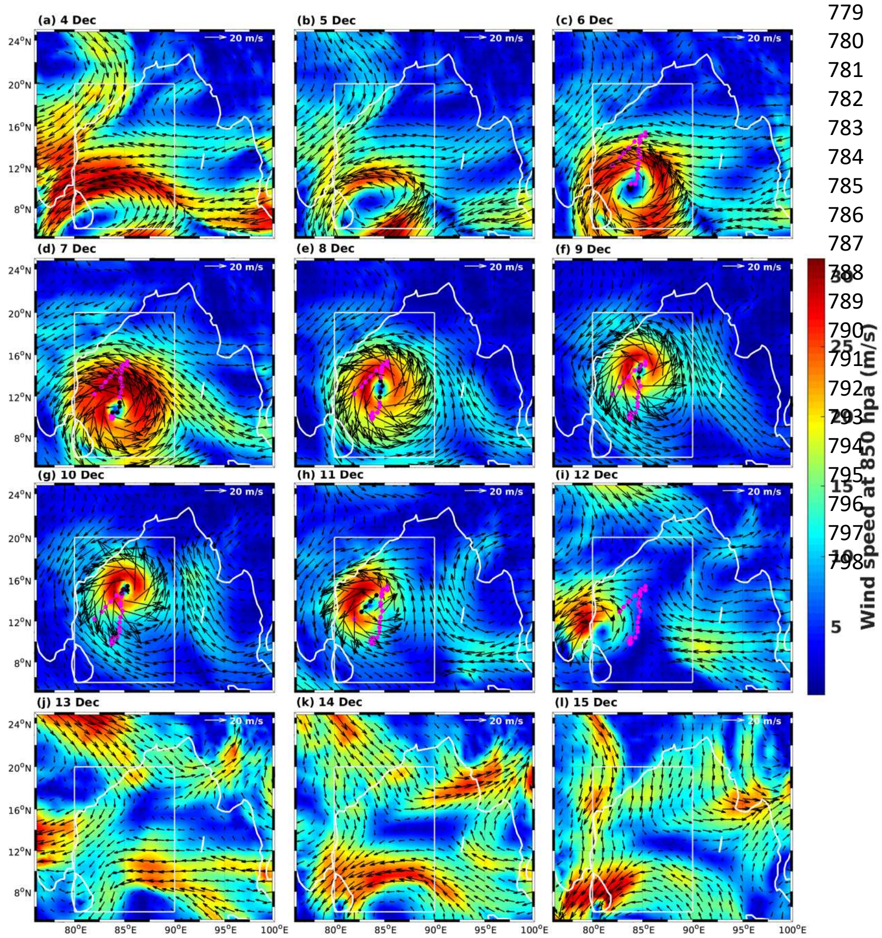

Figure 4 Spatial maps of wind speed (shading, m/s) overlaid with wind vectors (thin arrow) at 850 hpa from 4th (a) to 15th (l) December 2013 with track of the cyclone overlaid. The black filled circles represent the position of the cyclone on a particular day, while the magenta filled circles indicate the track.

Ocean Sci. Discuss., https://doi.org/10.5194/os-2018-133
Manuscript under review for journal Ocean Sci.
Discussion started: 28 January 2019

Ocean Science
Discussions
Open Access

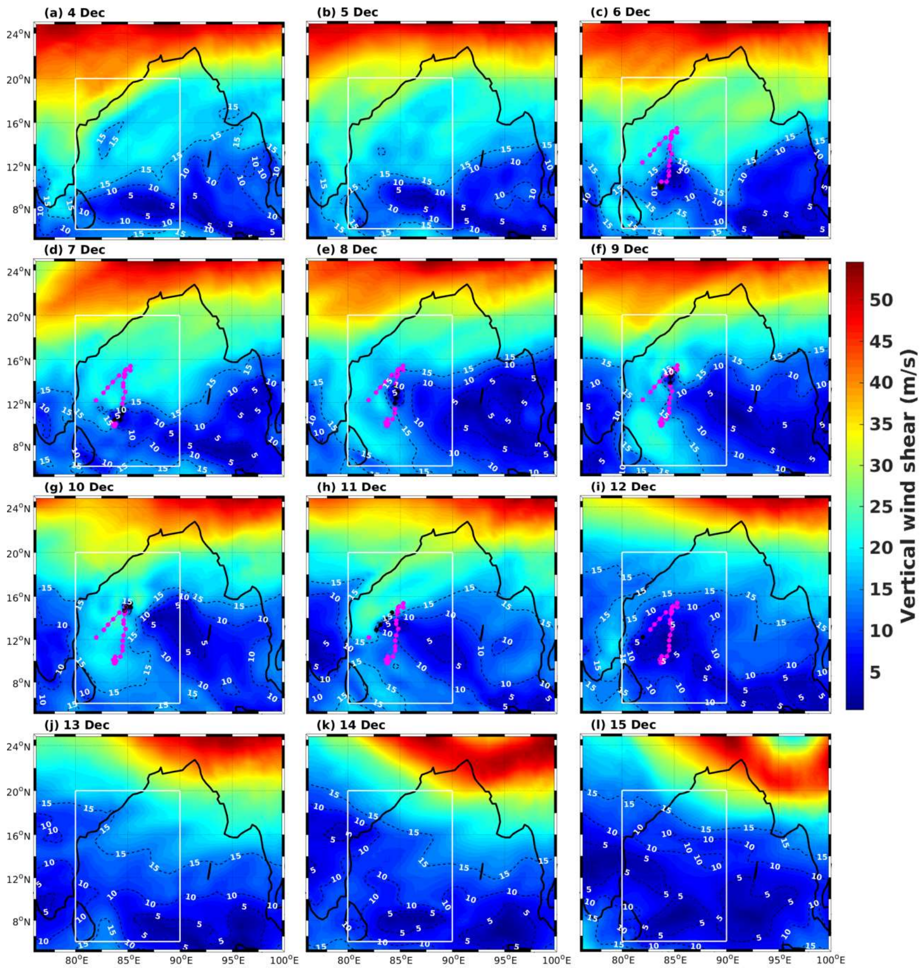

Figure 5 Spatial maps of vertical wind velocity difference between the 850 and 200hPa (shading, m/s) from 4th (a) to 15th (l) December 2013 with track of the cyclone overlaid. The black filled circles represent the position of the cyclone on a particular day, while the magenta filled circles indicate the track.

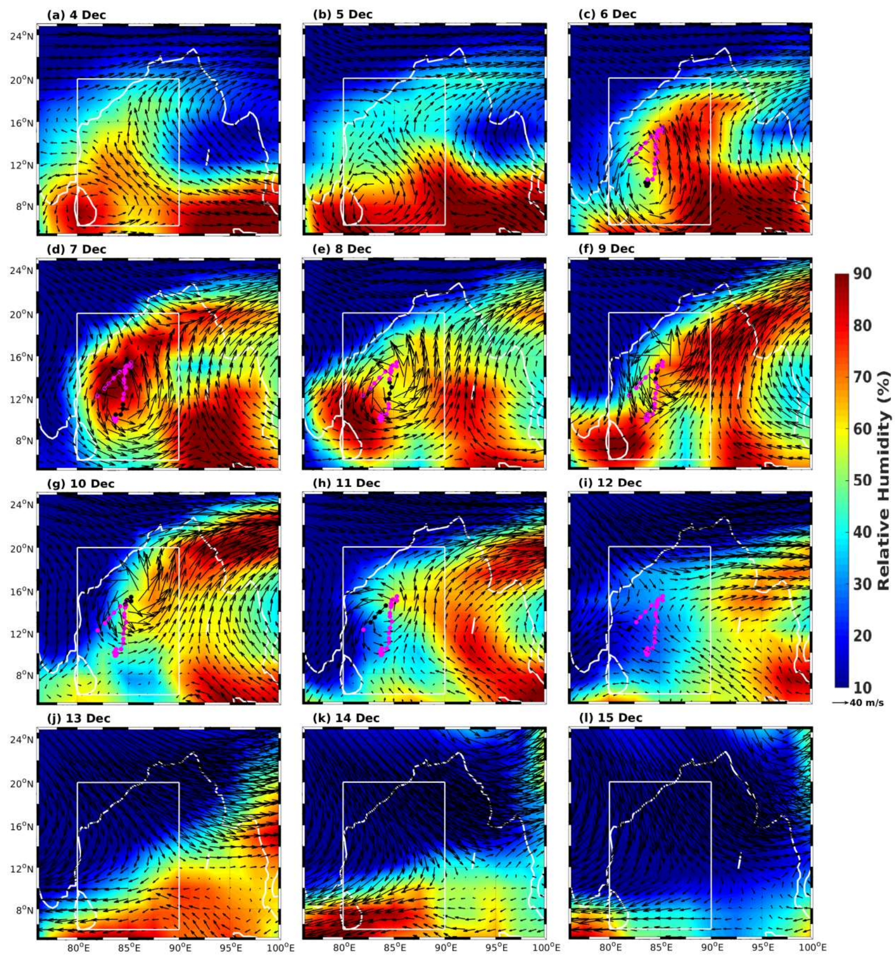

Figure 6 Spatial maps of relative humidity (%) overlaid with winds at mid-troposhere (500 hpa) from 4th (a) to 15th (l) December 2013 with track of the cyclone overlaid. The black filled circles represent the position of the cyclone on a particular day, while the magenta filled circles indicate the track.

Ocean Sci. Discuss., https://doi.org/10.5194/os-2018-133
Manuscript under review for journal Ocean Sci.
Discussion started: 28 January 2019

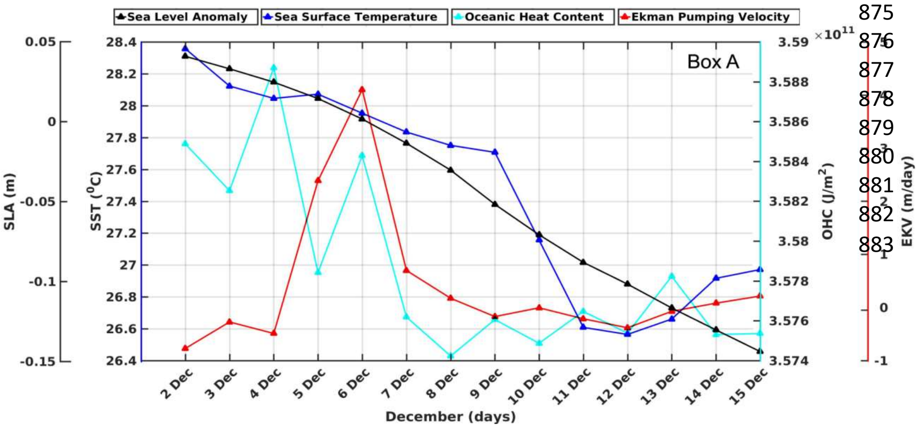

Figure 7 Space-averaged variation of the sea surface temperature (SST, ^{o}C), Ekman pumping velocity (EKV, m/day, positive upward), oceanic heat content (OHC, x 10^{11} J/m^2) and sea level anomaly (SLA, m) in Box A from 2-15 December 2013.

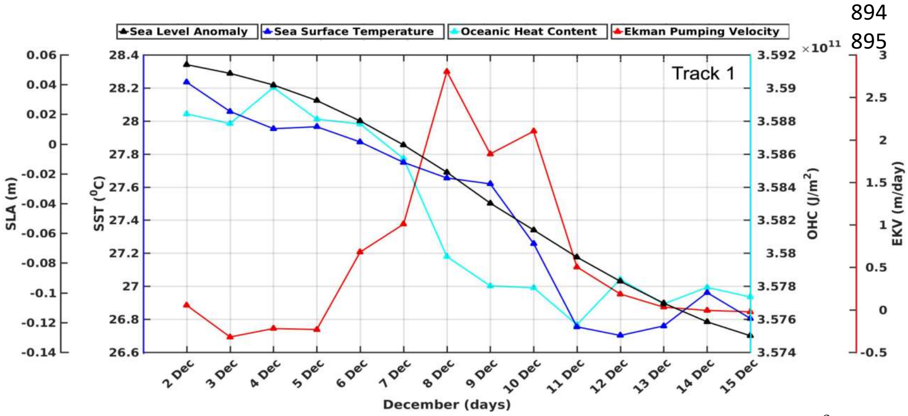

Figure 8 Along track variation of the sea surface temperature (SST, ^{o}C), Ekman pumping velocity (EKV, m/day, positive upward), oceanic heat content (OHC, x 10^{11} J/m^2) and sea level anomaly (SLA, m) along Track 1 from 2-15 December 2013. These are daily averages along the track.

Ocean Sci. Discuss., https://doi.org/10.5194/os-2018-133
Manuscript under review for journal Ocean Sci.
Discussion started: 28 January 2019

Ocean Science
Discussions
Open Access

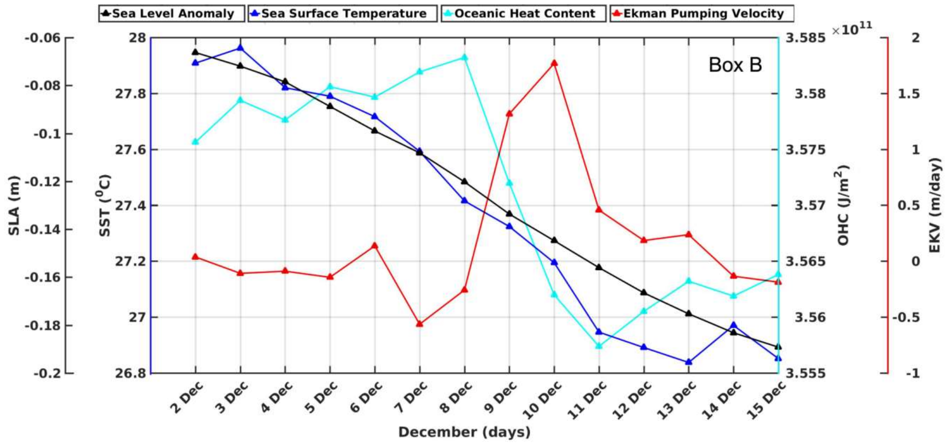

Figure 9 Space-averaged variation of the sea surface temperature (SST, °C), Ekman pumping velocity (EKV, m/day, positive upward), oceanic heat content (OHC, x 10^{11} J/m^2) and sea level anomaly (SLA, m) in Box B from 2-15 December 2013.

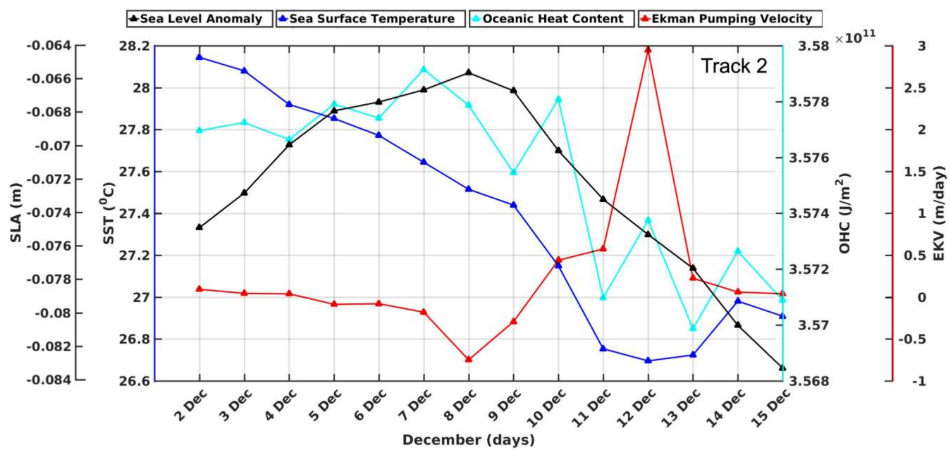

Figure 10 Along track variation of the sea surface temperature (SST, °C), Ekman pumping velocity (EKV, m/day, positive upward), oceanic heat content (OHC, x 10^{11} J/m^2) and sea level anomaly (SLA, m) along Track 2 from 2-15 December 2013. These are daily averages along the track.

Ocean Sci. Discuss., https://doi.org/10.5194/os-2018-133
Manuscript under review for journal Ocean Sci.
Discussion started: 28 January 2019

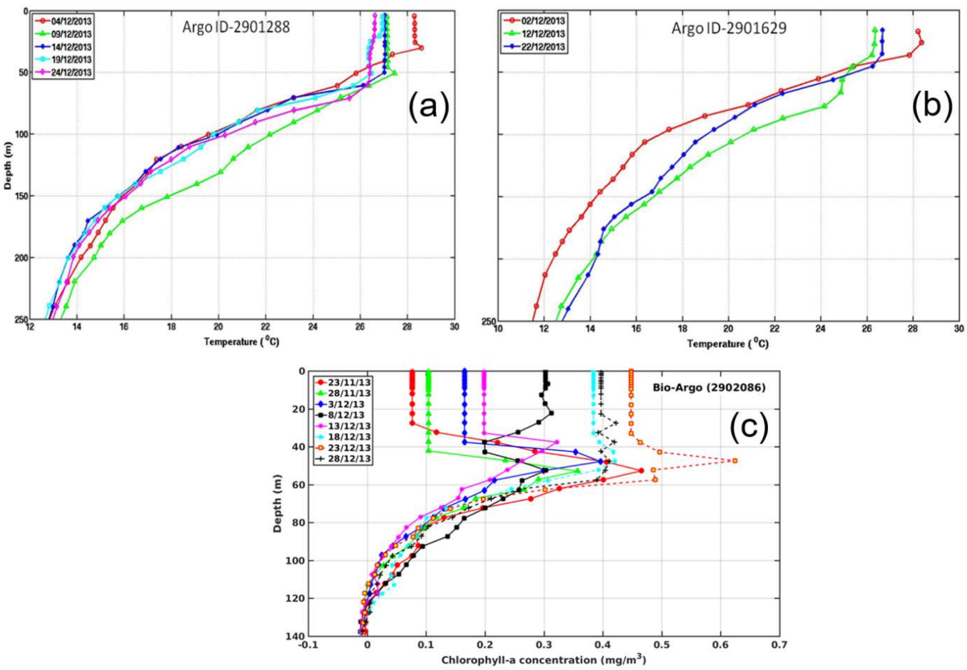

Figure 11 Time-series of the vertical profiles of temperature (°C) in the vicinity of Track 2 obtained from (a) Argo float ID-2901288 for 4, 9, 14, 19 and 24 December 2013, (b) Argo float ID-2901629 for 2, 12 and 22 December 2013 and (c) chlorophyll *a* (mg/m^3) in the vicinity of Track 1 obtained from Bio-Argo ID-2902086 for 23 and 28 November and 3, 8, 13, 18, 23 and 28 December 2013.

Ocean Sci. Discuss., https://doi.org/10.5194/os-2018-133
Manuscript under review for journal Ocean Sci.
Discussion started: 28 January 2019

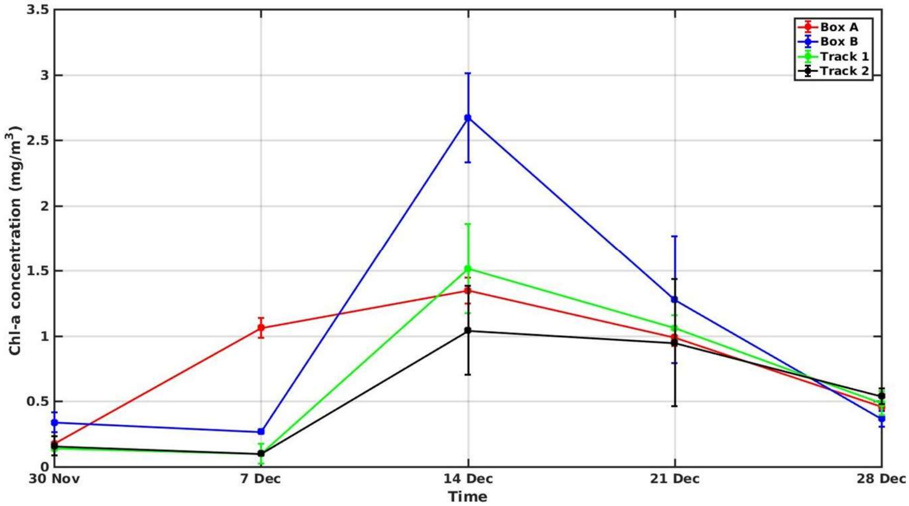

Figure 12 Time variation of weekly composite of chlorophyll *a* pigment concentrations (Chl-*a*, mg/m^3) in the Box A (red) and B (blue) and along Track 1 (green) and 2 (black) from 30 November to 28 December 2013. The vertical lines are the standard deviations.

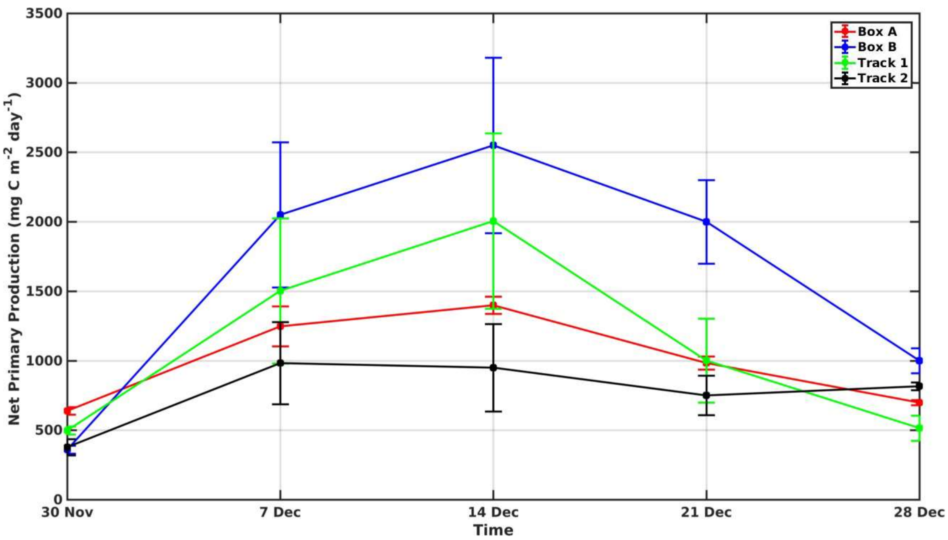

Figure 13 Time variation of weekly composite of net primary production (NPP, mg C m^{-2} day^{-1}) in the Box A (red) and B (blue) and along Track 1 (green) and 2 (black) from 30 November to 28 December 2013. The vertical lines are the standard deviations.

Ocean Sci. Discuss., https://doi.org/10.5194/os-2018-133
Manuscript under review for journal Ocean Sci.
Discussion started: 28 January 2019

Ocean Science
Discussions

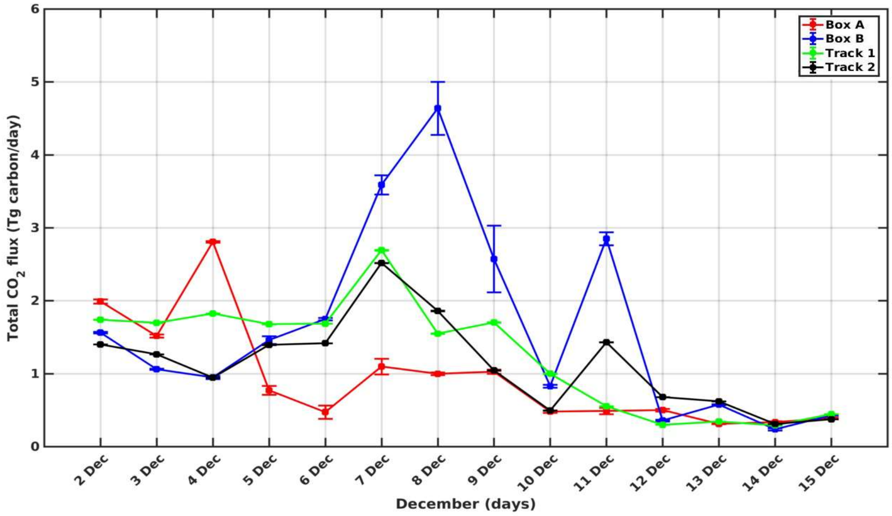

Figure 14 Daily variation total CO_2 flux (terra gram carbon per day) in the Box A (red) and B (blue) and along Track 1 (green) and 2 (black) from 2 to 15 December 2013. The vertical lines are the standard deviations.